

Influence of oxygen addition on the discharge characteristics of an argon plasma jet at atmospheric pressure

Junyu Chen(陈俊宇), Na Zhao(赵娜), Jiacun Wu(武珈存), Kaiyue Wu(吴凯玥), Furong Zhang(张芙蓉), Junxia Ran(冉俊霞), Pengying Jia(贾鹏英), Xuexia Pang(庞学霞), and Xuechen Li(李雪辰)

Citation: Chin. Phys. B, 2022, 31 (**6**): 065205. DOI: 10.1088/1674-1056/ac601a
Journal homepage: http://cpb.iphy.ac.cn; http://iopscience.iop.org/cpb

What follows is a list of articles you may be interested in

Sterilization of mycete attached on the unearthed silk fabrics by an atmospheric pressure plasma jet

Rui Zhang(张锐), Jin-song Yu(於劲松), Jun Huang(黄骏), Guang-liang Chen(陈光良), Xin Liu(刘欣), Wei Chen(陈维), Xing-quan Wang(王兴权), Chao-rong Li(李超荣)
Chin. Phys. B, 2018, 27 (**5**): 055207. DOI: 10.1088/1674-1056/27/5/055207

Characteristic plume morphologies of atmospheric Ar and He plasma jets excited by a pulsed microwave hairpin resonator

Zhao-Quan Chen(陈兆权), Ben-Kuan Zhou(周本宽), Huang Zhang(张煌), Ling-Li Hong(洪伶俐), Chang-Lin Zou(邹长林), Ping Li(李平), Wei-Dong Zhao(赵卫东), Xiao-Dong Liu(刘晓东), Olga Stepanova, A A Kudryavtsev
Chin. Phys. B, 2018, 27 (**5**): 055202. DOI: 10.1088/1674-1056/27/5/055202

Characteristics of helium DC plasma jets at atmospheric pressure with multiple cathodes

Cheng Wang(王城), Zelong Zhang(张泽龙), Haichao Cui(崔海超), Weiluo Xia(夏维珞), Weidong Xia(夏维东)
Chin. Phys. B, 2017, 26 (**8**): 085207. DOI: 10.1088/1674-1056/26/8/085207

LIF diagnostics of hydroxyl radical in a methanol containing atmospheric-pressure plasma jet

Mu-Yang Qian(钱沐杨), San-Qiu Liu(刘三秋), Xue-Kai Pei(裴学凯), Xin-Pei Lu(卢新培), Jia-Liang Zhang(张家良), De-Zhen Wang(王德真)
Chin. Phys. B, 2016, 25 (**10**): 105205. DOI: 10.1088/1674-1056/25/10/105205

Pulsed microwave-driven argon plasma jet with distinctive plume patterns resonantly excited by surface plasmon polaritons

Chen Zhao-Quan, Yin Zhi-Xiang, Xia Guang-Qing, Hong Ling-Li, Hu Ye-Lin, Liu Ming-Hai, Hu Xi-Wei, A. A. Kudryavtsev
Chin. Phys. B, 2015, 24 (**2**): 025203. DOI: 10.1088/1674-1056/24/2/025203

Influence of oxygen addition on the discharge characteristics of an argon plasma jet at atmospheric pressure

Junyu Chen(陈俊宇)[1], Na Zhao(赵娜)[1,2], Jiacun Wu(武珈存)[1], Kaiyue Wu(吴凯玥)[1], Furong Zhang(张芙蓉)[1], Junxia Ran(冉俊霞)[1], Pengying Jia(贾鹏英)[3], Xuexia Pang(庞学霞)[3], and Xuechen Li(李雪辰)[1,3,†]

[1] *College of Physics Science & Technology, Hebei University, Baoding* 071002, *China*
[2] *School of Mathematics and Physics, Handan University, Handan* 056005, *China*
[3] *Institute of Life Science & Green Development, Hebei University, Baoding* 071002, *China*

(Received 24 January 2022; revised manuscript received 22 February 2022; accepted manuscript online 23 March 2022)

Plasma jet is an important low-temperature plasma source in extensive application fields. To promote the production of active oxygen species, oxygen is often introduced into the inert working gas. However, the influence of oxygen content on the discharge characteristics of an argon plasma jet is not clear. Aim to this status, an argon plasma jet in a single-electrode geometry is employed to investigate the influence of oxygen concentration (C_O) on discharge aspects. Results indicate that with increasing C_O ($\leq 0.6\%$), the plume transits from a diffuse morphology to a hollow structure. Electrical and optical measurements reveal that both discharge number per voltage cycle and pulse intensity alter with varying C_O. Moreover, discharge morphologies of negative and positive discharges obtained by fast photograph also shift with varying C_O. Besides, optical emission spectra are collected to investigate atomic C_O, electron density, and electron temperature. The results mentioned above are explained qualitatively, which are believed to be of great significance for the applications of atmospheric pressure plasma jet.

Keywords: plasma jet, oxygen addition, fast photography, optical emission spectra

PACS: 52.80.Tn, 52.50.Dg, 52.70.Kz **DOI:** 10.1088/1674-1056/ac601a

1. Introduction

Without the need for any vacuum device, atmospheric pressure plasma jet can produce a kind of remote plasma in open atmosphere, which is also referred to as a plasma plume. Being abundant with active species in plasma plume,[1,2] plasma jet has extensive applications, such as material synthesis,[3–5] surface modification,[6–8] ozone generation,[9] water purification,[10] methane conversion,[11] sterilization,[12–14] catalysis,[15] and medicine.[16,17]

For an inert-gas plasma jet in a barrier discharge configuration, three distinct operating modes are witnessed with varying input power, which include a chaotic mode, a bullet one, and a continuous one.[18] For the plasma jet operated in the bullet mode, a fast-moving bullet-like plasma is observed in plasma plume when imaged by fast photography.[19] The formation of plasma bullet is attributed to a streamer regime.[20] In addition to discharge regime, various discharge characteristics, such as plume length,[21–24] plume morphology,[25–30] and plasma parameters,[27–29,31–33] are investigated for inert-gas plasma jet.

In fact, oxygen is often added to promote the production of active species,[34] thus increasing the plasma treatment efficiency.[35] However, oxygen addition is harmful for plume length.[36,37] Besides, vibrational and gas temperatures increase with increasing oxygen content of a helium jet.[37] Due to the electronegativity of oxygen molecules, electron density decreases with increasing oxygen content of a helium jet.[38] For low-cost argon plasma jet,[39,40] a constant oxygen dose has been investigated.[41–43] In fact, discharge aspects are influenced by oxygen concentration (C_O). Preliminary results have revealed that C_O affects plume length,[36,37] electron density and gas temperature.[37,38] Detailed investigations are needed for the influence of C_O on the discharge characteristic of an argon plasma jet.

In this paper, a single-electrode argon plasma jet is employed to investigate in detail the influence of oxygen addition on the discharge characteristics including plume morphology, discharge intensity, atomic oxygen concentration, electron density and electron temperature.

2. Experimental setup

The plasma jet is in a single-electrode geometry, whose schematic diagram is drawn in Fig. 1. A 12.0 cm long tungsten needle (both radius and tip radius are 0.5 mm) is poised at the axis of a quartz tube with inner and outer diameters of 5.0 mm and 8.0 mm, respectively. The needle tip is aligned with the quartz-tube nozzle. Argon and oxygen, both of which have a purity of 99.999%, are regulated by two independent gas flow meters (Sevenstar CS200A). Hence, oxygen content (C_O, volume ratio) in argon is variable with a total flow rate (Q). A homemade power source that produces a sinusoidal voltage with an amplitude (V_p) of 10.0 kV

†Corresponding author. E-mail: plasmalab@126.com; xcli@mail.hbu.edu.cn
© 2022 Chinese Physical Society and IOP Publishing Ltd

and a frequency (f) of 3.0 kHz is electrically connected with the plasma jet. The voltage is detected by a probe (Tektronix P6015A). A lens is used to focus integrated light emitted from the jet, which is then collected by a photomultiplier tube (PMT) (ET 9130/100B). Utilizing a 4-channel digital oscilloscope (Tektronix DPO4104), waveforms of applied voltage and integrated light signal can be simultaneously obtained. In addition, a digital camera (Canon EOS 5D Mark IV) and an electron-multiplying intensified charge-coupled device (emICCD, PI MAX4) are utilized to capture the plume images. A spectrometer (ACTON SP2750) installed with an emICCD (PI MAX4) at the outlet slit is used to collect optical emission spectrum. A maximal spectral resolution is realized with a grating of 2400 grooves/mm. Temporally resolved spectrum is obtained with a method similar to that reported previously by us.[30] A TTL signal to trigger the emICCD is displayed along with the light emission signal by the digital oscilloscope. Hence, the optical gate of the emICCD is presented on the oscilloscope with reference to the discharge. Through varying the gate time, temporally resolved spectra can be obtained. The spatially resolved spectrum is realized by varying the detection position of an optical fiber connecting with the entrance slit of the spectrometer.

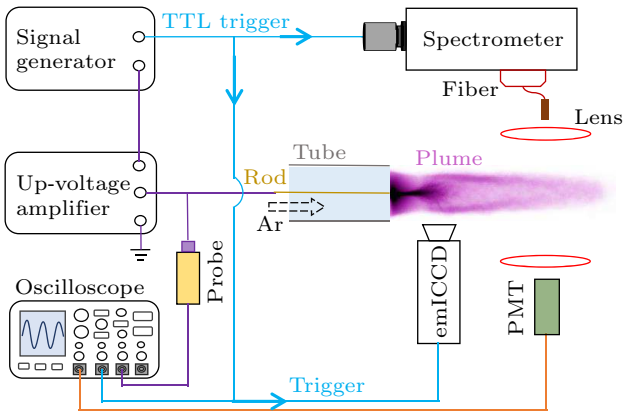


Fig. 1. Schematic diagram of the experimental setup.

3. Results and discussion

Images of the argon plume are presented in Fig. 2 with varying C_O. When the working gas is pure argon ($C_O = 0$), the plasma jet emanates a solid plume, which is composed of a white part and a purple one from side-view images (left row). The white part shortens with increasing C_O (0.2% to 0.4%). However, the length of the whole plume keeps almost constant with varying C_O in the small range. The purple part is diffuse, which transits to a hollow void when C_O reaches 0.6%. The morphology transition is observed more clearly from the front-view images (right row). Here, the central spot comes from the white part. Obviously, the cross section of the focus plane is diffuse with a low C_O. A purple ring resulting from the hollow structure is observed with C_O of 0.6%. In brief, there is a transition from a diffuse morphology to a hollow structure with increasing C_O.

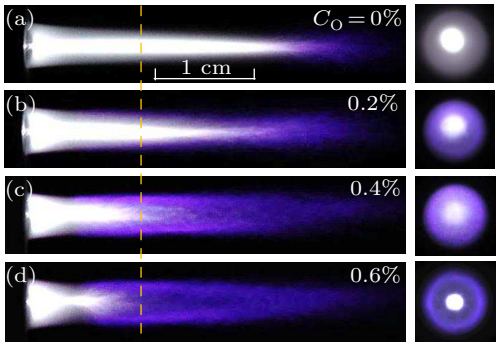


Fig. 2. Side-view (left) and front-view (right) images with varying C_O. The front-view images are focused at the dashed line (10 mm from the jet nozzle). Other parameters are $V_p = 10.0$ kV, $f = 3.0$ kHz, $Q = 4.0$ L/min, and $t_{exp} = 0.1$ s.

Figure 3 illustrates waveforms of applied voltage and light emission signal from the plasma plume with varying C_O. For the sake of convenience, we define positive discharge and negative one, which correspond to the discharges initiating at positive negative voltages, respectively. When the working gas is pure argon, some positive and negative discharges appear under V_p of 10.0 kV, which is similar to that reported by Ouyang *et al.*[44] With increasing C_O (0.2% and 0.4%), the number of positive and negative discharges decreases per voltage cycle. At the same time, the maximal intensity of positive discharges increases, while that of negative ones decreases. For the hollow plume ($C_O = 0.6\%$), one can see that only one positive discharge initiates per voltage cycle and negative discharge is almost ignorable.

Fast photography implemented by an ICCD was often used to reveal the propagation of streamers in a plasma jet.[1] Through using the emICCD that has a higher amplification than ICCD, negative discharge and positive one with varying C_O are imaged, as illustrated in Fig. 4. Discharge duration is around 300 ns, and t_{exp} of 1.0 μs is used to capture single discharge image in Fig. 4. Apparently, diffuse negative discharge extends along the argon channel, which looks like a cone. With increasing C_O, the length of the cone decreases. In contrast to the cone-like discharge, positive discharge is slimmer. The left side seems like a thin column, which appears mainly at the axis of the argon stream. The right side tends to be stochastically branched. Moreover, the thin column shortens and the branched part lengthens with increasing C_O. When C_O reaches 0.6%, the branches appear at the boundary layer of the argon channel (or the interface between the argon stream and the surrounding air),[27] which results in the hollow structure of the plume. From Fig. 4, it can be found that negative and positive discharges contribute to the white and purple parts of the argon plume, respectively.

Figure 5 illustrates 300 nm to 900 nm scanned optical emission spectra of the argon plasma plume. The spectra mainly include the lines from OH ($A^2\Sigma^+ \rightarrow X^2\Pi$) at

308.9 nm,[45] and those from the second positive system of N_2 ($C^3\Pi_u \rightarrow B^3\Pi_g$).[46] Both of them come from the diffusion of H_2O and N_2 in ambient air.[47,48] Besides, there are lots of spectral lines of Ar I ($2p_3 \rightarrow 1s_4$, 738.4 nm; $2p_1 \rightarrow 1s_2$, 750.4 nm; $2p_6 \rightarrow 1s_5$, 763.7 nm; $2p_2 \rightarrow 1s_3$, 772.7 nm) from the $4p \rightarrow 4s$ transitions, which are clearly presented in the spectra.[49] Moreover, the dissociation of oxygen molecule contributes to atomic oxygen emission at 844.6 nm.[50]

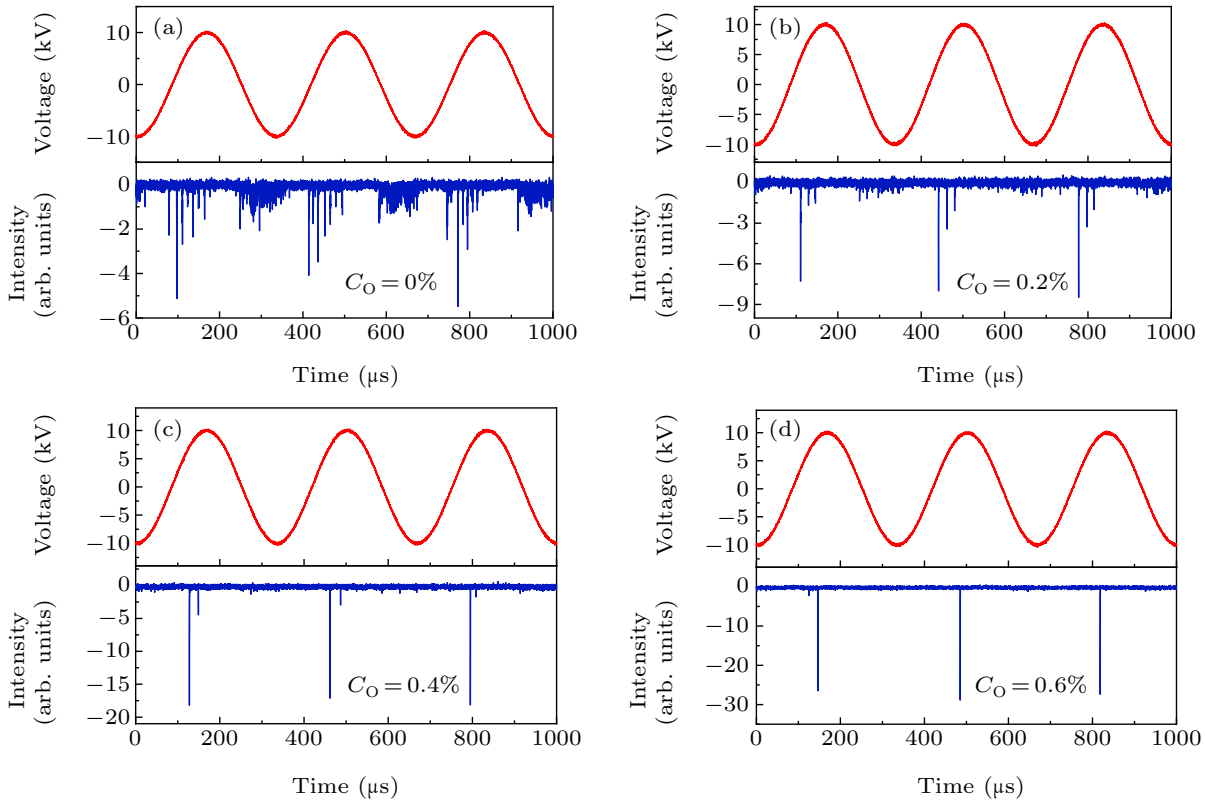


Fig. 3. Waveforms of applied voltage and integrated emission signal from the plasma jet. Panels (a)–(d) correspond to Figs. 2(a)–2(d), respectively.

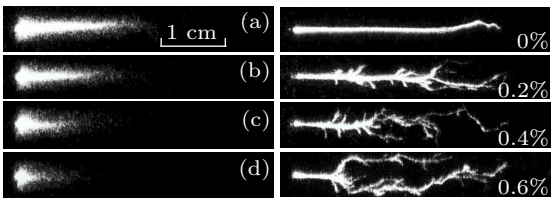


Fig. 4. Single-shot emICCD images exposed to a negative discharge (left) and a positive discharge (right) of the plasma jet with varying C_O.

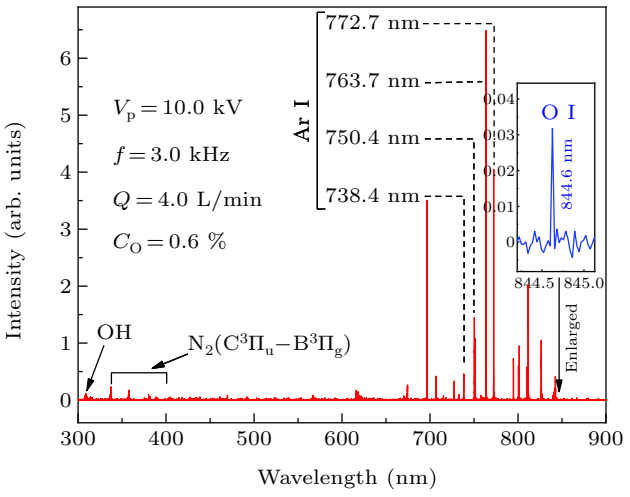


Fig. 5. The 300 nm to 900 nm scanned spectrum emitted from the plasma plume.

Optical actinometry is used to investigate atomic C_O, which is positively related with intensity ratio of the spectral lines (844.6 nm to 750.4 nm) in a small range of C_O.[21,51] From temporally and spatially resolved spectra, the spatial distribution of atomic C_O can be obtained for negative discharge and positive one, respectively, as indicated in Fig. 6. Figure 6 reveals that with increasing C_O, averaged atomic oxygen concentration (reflected by the intensity ratio) increases for both positive and negative discharges. Compared with that of negative discharge, atomic oxygen concentration of positive discharge is higher. Atomic C_O increases with increasing distance away from the needle tip. The above mentioned phenomenon can be explained as follows.

With increasing C_O, more oxygen molecules participate in the discharge process, leading to the production of more oxygen atoms by electron impact dissociation.[21] As a result, atomic C_O increases as C_O increases. On account of the same reason, more oxygen molecules that diffuse into the working gas contribute to the growing atomic C_O with increasing distance from the needle tip. Moreover, the difference of atomic C_O between negative discharge and positive one may come from their different plasma parameters (density and temperature of electrons), which will be shown later. With lower

plasma parameters, less oxygen molecules will be dissociated by electron impact, leading to lower atomic C_O in negative discharge.

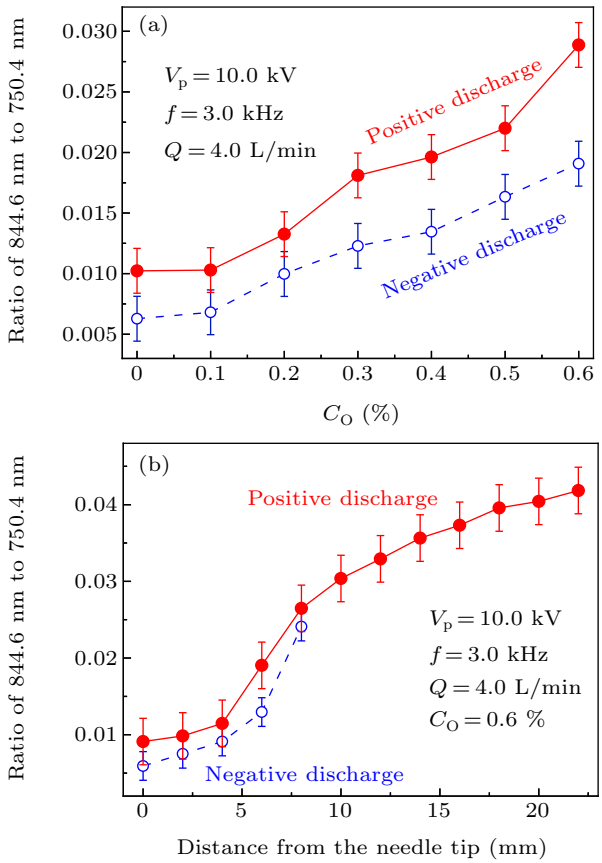


Fig. 6. (a) Intensity ratio of spectral lines (844.6 nm to 750.4 nm) as a function of C_O. (b) Spatial distribution of intensity ratio (844.6 nm to 750.4 nm) along the argon channel.

Intensity ratios of spectral lines can reflect plasma parameters,[52] such as density and temperature for electrons.[49,53] The line intensity ratios (738.4 nm to 763.7 nm, positively related with electron density) and (763.7 nm to 772.7 nm, positively related with electron temperature) as functions of C_O are shown in Fig. 7. Here, intensity ratios are calculated from integrated spectra, which reflect space-averaged density and temperature of electrons. Apparently, with increasing C_O, average electron density (reflected by the ratio of 738.4 nm to 763.7 nm) presents a decreasing tendency, while average electron temperature (the ratio of 763.7 nm to 772.7 nm) increases. Compared with those of negative discharge, average density and temperature of electrons are higher for positive discharge.

As is well known, both negative and positive discharges of plasma jet operate in a streamer regime.[1,20,24,27–30,54] Compared with negative discharge (anode-directed streamer), positive discharge (cathode-directed streamer) has a higher electric field strength (E).[29,55] Electrons are mainly produced in the plasma through the impact of argon atoms by electrons, which is dominated by the first Townsend ionization coefficient (α).[56,57] α is a function of E.[58] A higher E tends to produce a plasma with a higher electron density. Therefore, positive discharge has a higher electron density than negative discharge. Besides, electron temperature depends on E because electrons obtain more energy in one mean free path under a stronger E. Hence, a plasma with a higher electron temperature can be generated with a higher E.[59] Due to the discrepancy of E, negative discharge is lower than positive one in plasma parameters (density and temperature of electrons).

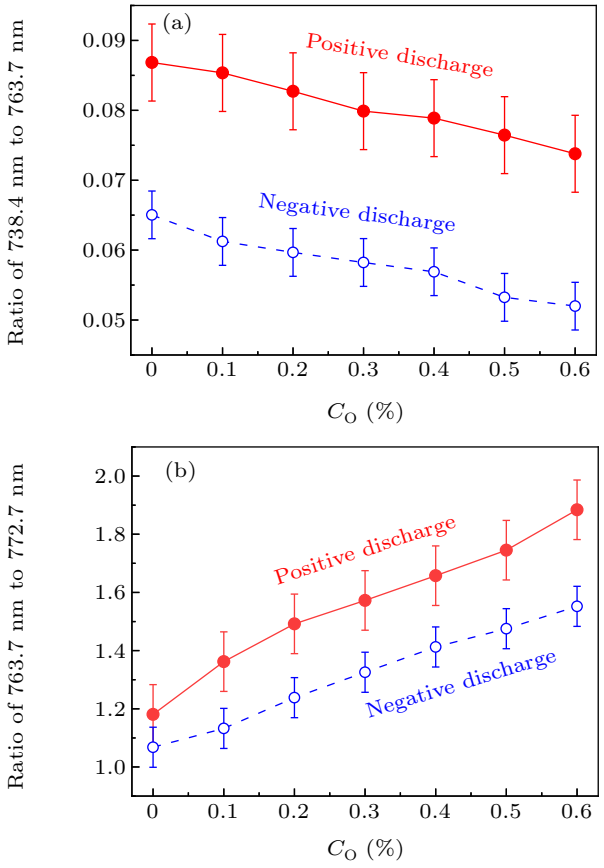


Fig. 7. Intensity ratios of spectral lines (738.4 nm to 763.7 nm) (a) and (763.7 nm to 772.7 nm) (b) as functions of CO. $V_p = 10.0$ kV, $f = 3.0$ kHz, and $Q = 4.0$ L/min.

Long-life active species, such as metastable argon atoms (Ar^*), play an important role in gas discharge.[60] Since residual Ar^* can greatly decrease the field threshold for breakdown (E_{th}) due to stepwise ionization,[60] which is described by the following reactions:

$$e + Ar \rightarrow e + Ar^*, \quad (1)$$

$$e + Ar^* \rightarrow Ar^+ + 2e, \quad (2)$$

where e = electron, Ar = ground state argon atom, and Ar^+ = positive argon ion. Consequently, the forthcoming discharge is inclined to initiate in the argon channel abundant with Ar^*. Resultantly, negative discharge always extends along and covers the left side of the argon channel because the previous discharge (positive discharge) distributes the channel axis with Ar^*. Based on the same reason, the left side of positive discharge appears in the axis of the argon stream because abun-

dant residual Ar^* are concentrated in the axis, which result from the previous positive and negative discharges.

Compared with the left side, more oxygen molecules exist at the right side of the argon stream due to the diffusion of ambient air. Oxygen molecules can quench Ar^* through the following reaction:[60,61]

$$Ar^* + O_2 \rightarrow Ar + O_2. \quad (3)$$

Therefore, the right side of the argon stream has a lower concentration of Ar^*. As a result, a positive discharge can only be initiated under a stronger E at the right side. Numerical simulation has revealed that streamer bifurcates under a stronger field.[62] Consequently, the right side of positive discharge is branched. With increasing C_O of the working gas, more residual Ar^* will be quenched,[26,61] leading to a higher E_{th} of the argon stream. This leads to the shortening column and lengthening branched part of positive discharge. In fact, the argon stream is surrounded by negative oxygen ions,[63] which can provide the forthcoming discharge with seed electrons through detachment. This factor will decrease E_{th} of the boundary layer. With the increased E_{th} of the argon stream and the reduced E_{th} in the interfacial layer, discharge tends to appear in the interfacial layer when C_O reaches a certain value (0.6%).

As mentioned above, E_{th} monotonously increases with increasing C_O. This means that discharge will initiate under a stronger E with a higher C_O. Since electron temperature depends on E, electron temperature is higher under a stronger E. Hence, electron temperature increases for both negative and positive discharges with increasing C_O. Coefficient α is not only a function of E, but also related with gas ingredient.[55] The quenching of Ar^* by oxygen molecules decreases the number of electrons produced by stepwise ionization, thus decreasing α coefficient.[60] Moreover, some electrons are attached by oxygen molecules, which also decrease electron density in the plasma. Consequently, electron density decreases for both positive and negative discharges with increasing C_O.

4. Conclusion

In this paper, the influence of oxygen addition on discharge characteristics has been investigated in detail for a single-electrode argon plasma jet. Within a small range of C_O ($\leq 0.6\%$), the emanated plasma plume keeps almost constant in length, which is composed of the left white and the right purple parts. With increasing C_O, the purple part transits from the diffuse morphology to a hollow void. During this process, the number of positive and negative discharges decreases per voltage cycle. At the same time, the maximal intensity shows an increasing trend for positive discharge, while a decreasing trend for negative one. Moreover, emICCD images reveal that negative discharge looks like a cone, while positive discharge is composed of a column and some branches. With increasing C_O, both the cone and the column turn shorter, however, the branches become longer. From optical emission spectra, atomic C_O, density and temperature of electrons are investigated as functions of C_O. Finally, these variation trends have been analyzed qualitatively.

Acknowledgments

Project supported by the National Natural Science Foundation of China (Grant Nos. 51977057 and 11875121), the Natural Science Foundation of Hebei Province, China (Grant Nos. A2020201025 and A2019201100), the Natural Science Interdisciplinary Research Program of Hebei University (Grant Nos. DXK202011 and DXK201908), Post-graduate's Innovation Fund Project of Hebei Province, China (Grant Nos. CXZZBS2019023 and CXZZBS2019029), and Post-graduate's Innovation Fund Project of Hebei University (Grant Nos. HBU2021ss063 and HBU2021bs011).

References

[1] Lu X P, Naidis G V, Laroussi M, Reuter S, Graves D B and Ostrikov K 2016 *Phys. Rep.* **630** 1
[2] Zhao N, Wu K Y, Chen J Y, Jia P Y and Li X C 2021 *Spectrosc. Spect. Anal.* **41** 2644
[3] Dou S, Tao L, Wang R L, Hankari S E, Chen R and Wang S Y 2018 *Adv. Mater.* **30** 1705850
[4] Zhang Y T, Guo Y, Wang D W, Feng Y and Ma T C 2010 *Chin. Phys. Lett.* **27** 068201
[5] Liu Y F, Han J M, Zhang G L, Wang J L, Li M, Yang W B, Liu C Z, Li H Q and Yang S Z 2004 *Chin. Phys. Lett.* **21** 1314
[6] Wang R X, Zhang C, Liu X, Xie Q, Yan P and Tao S 2015 *Appl. Surf. Sci.* **328** 509
[7] Wu J C, Wu K Y, Chen J Y, Song C H, Jia P Y and Li X C 2021 *Plasma Sci. Technol.* **23** 085504
[8] Shi Y C, Li J J, Liu H, Zuo Y G, Bai Y, Sun Z F, Ma D L and Chen G C 2015 *Chin. Phys. Lett.* **32** 088104
[9] Wu M, Uehara S, Wu J, Xiao Y C, Nakajima T and Sato T 2020 *J. Phys. D* **53** 485201
[10] Li X C, Wang B, Jia P Y, Yang L W, Li Y R and Chu J D 2017 *Plasma Sci. Technol.* **19** 115505
[11] Shao T, Wang R X, Zhang C and Yan P 2018 *High Volt.* **3** 14
[12] Nicol M J, Brubaker T R, Honish B J, Simmons A N, Kazemi A, Geissel M A, Whalen C T, Siedlecki C A, Bilén S G, Knecht S D and Kirimanjeswara G S 2020 *Sci. Rep.* **10** 3066
[13] Fan Z Q, Zhong J Y, Li Z W, Zheng Y C, Wang Z Z and Bai S P 2021 *J. Phys. D* **54** 455204
[14] Zhang R, Yu J S, Huang J, Chen G L, Liu X, Chen W, Wang X Q and Li C R 2018 *Chin. Phys. B* **27** 055207
[15] Ning W J, Dai D and Zhang Y H 2019 *Appl. Phys. Lett.* **114** 054104
[16] Athanasopoulos D, Svarnas P, Ladas S, Kennou S and Koutsoukos P 2018 *Appl. Phys. Lett.* **112** 213703
[17] Cheng C, Shen J, Xiao D Z, Xie H B, Lan Y, Fang S D, Meng Y D and Paul K C 2014 *Chin. Phys. B* **23** 075204
[18] Walsh J L, Iza F, Janson N B, Law V J and Kong M G 2010 *J. Phys. D* **43** 075201
[19] Teschke M, Kedzierski J, Finantu-Dinu E G, Korzec D and Engemann J 2005 *IEEE Trans. Plasma Sci.* **2** 310
[20] Lu X P and Laroussi M 2006 *J. Appl. Phys.* **100** 063302
[21] Li S Z, Huang W T, Zhang J L and Wang D Z 2009 *Appl. Phys. Lett.* **94** 111501
[22] Pinchuk M E, Stepanova O M, Astafiev A M, Lazukin A V and Chen Z Q 2019 *Appl. Phys. Lett.* **114** 194103
[23] Xiong Q, Lu X P, Ostrikov K, Xiong Z, Xian Y, Zhou F, Zou C, Hu J, Gong W and Jiang Z 2009 *Phys. Plasmas* **16** 043505

[24] Lu X P, Naidis G V, Laroussi M and Ostrikov K 2014 *Phys. Rep.* **540** 123
[25] Abdelaziz A A and Kim H H 2021 *Plasma Process. Polym.* **18** 2000190
[26] Abdelaziz A A, Teramoto Y and Kim H H 2022 *J. Phys. D* **55** 065201
[27] Li X C, Lin X T, Wu K Y, Jia P Y, Dong L F and Ran J X 2018 *Plasma Process. Polym.* **15** 1700224
[28] Li X C, Lin X T, Wu K Y, Ren C H, Liu R and Jia P Y 2019 *Plasma Sources Sci. Technol.* **28** 055006
[29] Li X C, Chen J Y, Lin X T, Wu J C, Wu K Y and Jia P Y 2020 *Plasma Sources Sci. Technol.* **29** 065015
[30] Wu J C, Jia P Y, Ran J X, Chen J Y, Zhang F R, Wu K Y, Zhao N, Ren C H, Yin Z Q and Li X C 2021 *Phys. Plasmas* **28** 073501
[31] Engeln R, Klarenaar B and Guaitella O 2020 *Plasma Sources Sci. Technol.* **29** 063001
[32] Li X C, Chen J Y, Wu K Y, Wu J C, Zhang F R, Zhao N, Jia P Y, Yin Z Q, Wang Y J and Ren C H 2021 *Phys. Plasmas* **28** 103507
[33] Zhao N, Wu K Y, He X R, Chen J Y, Tan X, Wu J C, Ran J X, Jia P Y and Li X C 2022 *J. Phys. D* **55** 015203
[34] Brisset A, Gibson A R, Schröter S, Niemi K, Booth J, Gans T, O'Connell D and Wagenaars E 2021 *J. Phys. D* **54** 285201
[35] Han X, Liu D X, Wang W T, Liu Z J, Guo L, Rong M Z and Kong M G 2018 *Phys. Plasmas* **25** 113506
[36] Fang Z, Zhou Y D and Yao Z Q 2014 *IEEE Trans. Plasma Sci.* **42** 2618
[37] Thiyagarajan M, Sarani A and Nicula C 2013 *J. Appl. Phys.* **113** 233302
[38] Kimura T and Noto M 2006 *J. Appl. Phys.* **100** 063303
[39] Li J, Lei B Y, Wang J, Xu B P, Ran S, Wang Y S, Zhang T Y, Tang J, Zhao W and Duan Y X 2021 *Commun. Phys.* **4** 64
[40] Fang Z, Ruan C, Shao T and Zhang C 2016 *Plasma Sources Sci. Technol.* **25** 01LT01
[41] Wang S, Schulz-von der Gathen V and Döbele H F 2003 *Appl. Phys. Lett.* **83** 3272
[42] Moravej M, Yang X and Hicks R F 2006 *J. Appl. Phys.* **99** 093305
[43] Lim J P and Uhm H S 2007 *Phys. Plasmas* **14** 093504
[44] Kong D L, He F, Yang B Y, Duan Z C, Han R Y, Miao J S, Yan X and Ouyang J T 2021 *J. Phys. D* **54** 405201
[45] Li X C, Jia P Y, Liu Z H, Li L C and Dong L F 2008 *Acta Phys. Sin.* **57** 1001 (in Chinese)
[46] Yang L J, Song C H, Zhao N, Zhou S, Wu J C and Jia P Y 2021 *Acta Phys. Sin.* **70** 155201 (in Chinese)
[47] Yuan Q H, Wang X M, Yin G Q, Li J and Dong C Z 2016 *Contrib. Plasma Phys.* **56** 870
[48] Xiong Q, Nikiforov A Y, Lu X P and Leys C 2010 *J. Phys. D* **43** 415201
[49] Zhu X M, Pu Y K, Balcon N and Boswell R 2009 *J. Phys. D* **42** 142003
[50] Greb A, Niemi K, O'Connell D and Gans T 2014 *Appl. Phys. Lett.* **105** 234105
[51] Wu J C, Wu K Y, Chen J Y, Song C H, Jia P Y and Li X C 2021 *Plasma Sci. Technol.* **23** 085504
[52] Li X C, Yuan N, Jia P Y, Chang Y Y and Ji Y F 2011 *Acta Phys. Sin.* **60** 125204 (in Chinese)
[53] Jiang W M, Tang J, Wang Y S, Zhao W and Duan Y X 2014 *Sci. Rep.* **4** 6323
[54] Li X C, Chang Y Y, Liu R F, Zhao H H and Di C 2013 *Acta Phys. Sin.* **62** 165205 (in Chinese)
[55] Starikovskiy A Y and Aleksandrov N L 2020 *Plasma Sources Sci. Technol.* **29** 075004
[56] Raizer Y P 1991 *Gas Discharge Physics* (Berlin: Springer)
[57] Li X C, Geng J L, Jia P Y, Wu K Y, Jia B Y and Kang P C 2018 *Acta Phys. Sin.* **67** 075201 (in Chinese)
[58] Jia P Y, Gao K, Zhou S, Chen J Y, Wu J C, Wu K Y and Li X C 2021 *Plasma Sources Sci. Technol.* **30** 095021
[59] Zhang B Y, Wang Q, Zhang G X and Liao S S 2014 *J. Appl. Phys.* **115** 043302
[60] Siefert N S, Sands B L and Ganguly B N 2006 *Appl. Phys. Lett.* **89** 011502
[61] Han D M, Liu Y X, Gao F, Liu W Y, Xu J and Wang Y N 2018 *Chin. Phys. B* **27** 065202
[62] Yuan X C, Li H W, Abbas M F, Li X R, Wang Z, Zhang G J and Sun A B 2020 *J. Phys. D* **53** 425204
[63] Ponomarev A A and Aleksandrov N L 2015 *Plasma Sources Sci. Technol.* **24** 035001